

Ionic Coulomb blockade as a fractional Wien effect

Nikita Kavokine , Sophie Marbach , Alessandro Siria and Lydéric Bocquet *

Recent advances in nanofluidics have allowed the exploration of ion transport down to molecular-scale confinement, yet artificial porins are still far from reaching the advanced functionalities of biological ion machinery. Achieving single ion transport that is tunable by an external gate—the ionic analogue of electronic Coulomb blockade—would open new avenues in this quest. However, an understanding of ionic Coulomb blockade beyond the electronic analogy is still lacking. Here, we show that the many-body dynamics of ions in a charged nanochannel result in quantized and strongly nonlinear ionic transport, in full agreement with molecular simulations. We find that ionic Coulomb blockade occurs when, upon sufficient confinement, oppositely charged ions form ‘Bjerrum pairs’, and the conduction proceeds through a mechanism reminiscent of Onsager’s Wien effect. Our findings open the way to novel nanofluidic functionalities, such as an ion pump based on ionic Coulomb blockade, inspired by its electronic counterpart.

Ionic transport is key to numerous processes, from neurotransmission to ultrafiltration^{1–4}. Over the past decade, it has been extensively investigated in biological systems, evidencing advanced functionalities such as high selectivity, ionic pumping and electrical or mechanical gating^{5–7}. However, it is only recently that experimental progress in nanoscience has allowed the fabrication of artificial pores with controlled material properties and channel- or slit-like geometries. These new systems have reached unprecedented nanometre- and even angstrom-scale confinements^{8–11}, yet they are still far from exhibiting the same functions as biological ionic machines.

At these scales, ion transport is usually described by the Poisson–Nernst–Planck (PNP) framework², which couples ion diffusive dynamics to electric interactions. Although it may account for nonlinear (for example, diode-type) effects², the PNP framework is intrinsically continuum and mean field. Building bio-inspired functions, however, may require control of transport at the single ion level, which is out of the reach of a mean-field description. Single charge transport in fact echoes the canonical Coulomb blockade (CB) phenomenon, which has been thoroughly explored in nanoelectronics. CB is typically observed in a single electron transistor: under fixed bias, the current between source and drain peaks at quantized values of the gating voltage¹². The origins of this effect stem from the many-body Coulomb interactions between electrons and from the discreteness of the charge carriers¹³. Similar physical ingredients are at play in a nanoscale channel filled with a salt solution (Fig. 1a): the ions also interact via Coulombic forces, and a variable surface charge on the channel walls can play the role of the gating voltage. One may therefore expect to observe an ‘ionic CB’, namely peaks in the ionic conductance of a nanochannel at quantized values of its surface charge. It is thus of interest that molecular dynamics simulations^{14–17} and experiments^{18–20} have shown what might be indirect signatures of ionic CB (although in the absence of a gating voltage), and conductance gating by a surface charge has been demonstrated in simulations of a biological ion channel model^{21,22}. These observations remain surprising, because ionic systems in water at room temperature have specific features contrasting with electronic systems that may preclude the occurrence of ionic CB. Beyond the absence of quantum effects, the fact that ions are of both signs—while electrons are only negative—results

in Debye screening, which is expected to greatly weaken the many-body interaction. It remains unclear under which conditions these aspects may suppress ionic transport quantization.

Although pioneering analytical efforts have translated the results established for electrons¹³ to the ionic case^{22–24}, a general theory for ionic CB, incorporating the unique features of ionic systems in contrast to their electronic counterparts, is still lacking. We develop such a theory in this Article.

Model definition and numerical results

Our theory is based on a simple but general model of a nanochannel which confines ions in one dimension (Fig. 1a). The channel has radius R and length $L \gg R$, as opposed to nanopores which have length $L \approx R$. The nanochannel is filled with water, which under confinement exhibits a priori an anisotropic dielectric permittivity $\bar{\epsilon}$ (refs. 25,26), and it is embedded in a membrane with low permittivity ϵ_m (whenever needed, we use $\epsilon_m = 2$). Under such conditions (Fig. 1b), the electric field lines produced by an ion stay confined inside the channel over a characteristic length ξ (ref. 27). This leads to a stronger Coulomb interaction than in the bulk solution, which is well described by the exponential potential

$$V(x) = k_B T \frac{\xi}{x_T} e^{-|x|/\xi} \quad (1)$$

This introduces a thermal length x_T (ref. 28), which quantifies the strength of the interaction. We detail in Supplementary Section 3 how the parameters ξ and x_T are related to the channel geometry and to the various dielectric constants. If the permittivity of confined water is assumed to be the same as in the bulk, one has $\xi \approx 7R$ and $x_T = R^2/2\ell_B$, where $\ell_B = 0.7$ nm is the Bjerrum length in bulk water. We shall use these relations in the following, keeping in mind that taking into account the anisotropic permittivity would result in a stronger interaction for a given confinement.

A charge is imposed on the confining surface and acts as a gate on the system; here, we reduce the surface charge to a point-like charge Q . The ions interact between themselves and with the surface charge through the potential given in equation (1); depending on conditions, an electric field E may be applied along the channel.

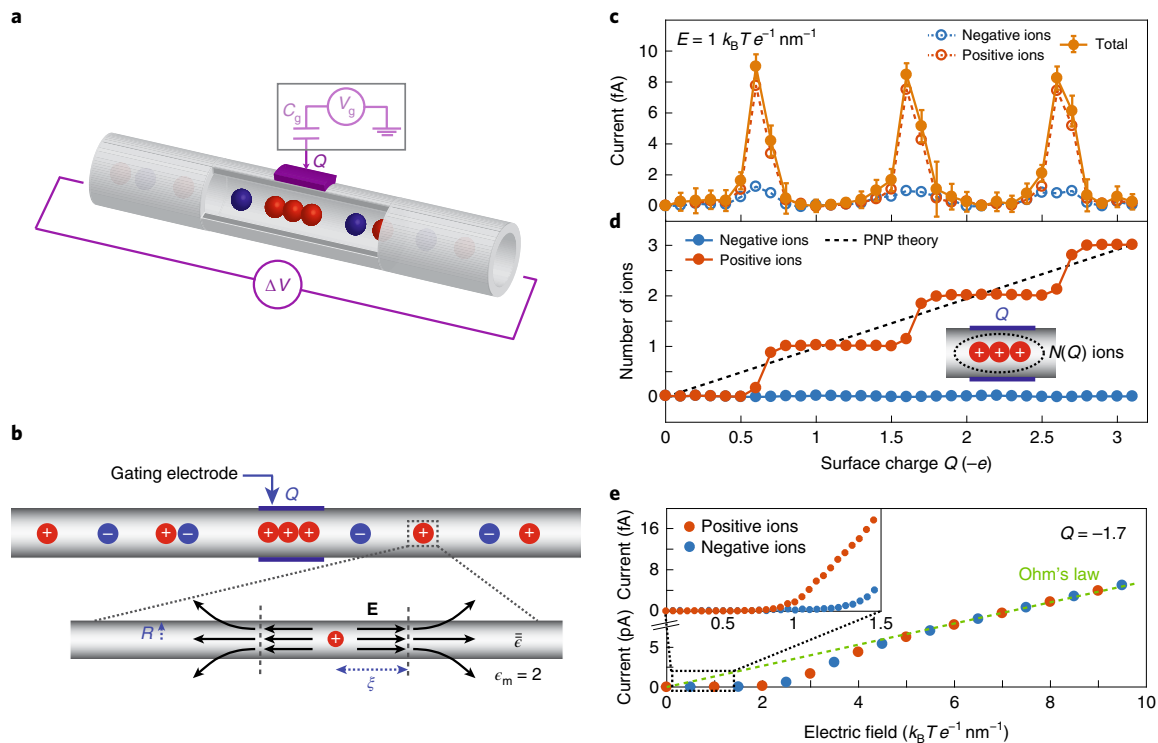


Fig. 1 | Brownian dynamics simulations of ionic CB in a nanochannel. **a**, Sketch of ions confined in a gated nanochannel. The tunable surface charge Q acts as a gate—it is equivalent to a voltage applied to an electrode, which is capacitively coupled to the channel. **b**, Setting for the Brownian dynamics simulations: the ions have quasi-1D Coulomb interactions, with the electric field confined in the channel over a characteristic length ξ . **c**, The ionic current through the channel, at fixed applied electric field ($E = 1 k_B T e^{-1} \text{ nm}^{-1}$), shows peaks at discrete values of the surface charge. **d**, The neutralizing charge $N(Q)$ —the total positive charge that screens the negative surface charge—increases in steps as a function of Q . The dashed line shows the mean-field prediction obtained from the equilibrium solution of the PNP equations (Supplementary Section 1.5), which is in complete disagreement with the simulations. **e**, Ionic current as a function of the applied electric field at fixed surface charge ($Q = -1.7$). A strongly nonlinear behaviour is observed. The parameters are thermal length $x_T = 0.09 \text{ nm}$, $\xi = 3.5 \text{ nm}$ and salt concentration $\rho_0 = 0.44 \text{ M}$. Error bars in **c–e** represent the standard deviation of the mean (smaller than the symbol size in **d**, **e**).

Before developing an analytical theory, we confirm using (grand canonical) Brownian dynamics simulations²⁹ that our simplified model displays the ionic CB phenomenology. Details of the simulations are provided in Supplementary Section 4: the measured quantities are the ionic current and the neutralizing charge $N(Q)$, defined as the total positive charge that screens the negative charge Q . Figure 1c,d shows typical simulation results. Remarkably, we do observe signatures of ionic CB: namely, the neutralizing charge $N(Q)$ is ‘quantized’, as it increases in discrete steps as a function of Q —this can be considered an equilibrium signature of ionic CB—and under an external electric field, the current peaks at discrete values of Q . We thus recover the same phenomenology as in simulations of nanopores^{21,22}, although in our general setting we do not assume electrostatic coupling between the channel entrances and the surface charge. Furthermore, our simulations reveal a very nonlinear current–voltage characteristic (Fig. 1e), with the conductance at low voltages being suppressed with respect to the conductance expected from Ohm’s law. Interestingly, the I – V characteristic for our ionic CB system differs from its electronic counterpart, where several steps in current versus applied voltage are observed before reaching Ohm’s law¹².

Fractional Wien effect theory

We now develop an analytical theory in order to understand this counterintuitive behaviour. The vision of CB in terms of energy barriers, which has been developed for electrons in quantum dots¹³ and adapted to ions in nanopores²², cannot apply here as

we consider a 1D nanochannel of arbitrary length. Moreover, the phenomenon at stake is clearly out of reach for the mean-field PNP equations^{1,2}. The PNP result for the neutralizing charge is derived in Supplementary Section 1.5 and shown in Fig. 1d. A perfectly linear behaviour for $N(Q)$ versus the surface charge Q is obtained, in contrast to the simulation results. Thus, the theoretical description of ionic CB requires us to exactly solve the underlying many-body problem.

To this end, we first compute the grand-canonical partition function of the confined electrolyte in the presence of the gating charge Q and with the pairwise interaction set by equation (1); the chemical potential is μ and the temperature T (we set $k_B T = 1$). The system under consideration closely resembles a 1D Coulomb gas model, which can be solved using a functional integral technique as in refs. 30–32, which we extend to incorporate an arbitrary gating charge density $q(x)$. An exhaustive calculation, reported in Supplementary Section 1.2, yields the partition function

$$\Xi = \int d\phi_0 d\phi_L e^{-x_T(\phi_0^2 + \phi_L^2)/4\xi} \mathcal{P}(\phi_L, L | \phi_0) \quad (2)$$

where the propagator $\mathcal{P}(\phi, x | \phi_0)$ solves

$$\frac{\partial \mathcal{P}}{\partial x} = \frac{1}{x_T} \frac{\partial^2 \mathcal{P}}{\partial \phi^2} + \left(iq\phi - \frac{x_T}{4\xi^2} \phi^2 + \frac{2z}{L} \cos \phi \right) \mathcal{P} \quad (3)$$

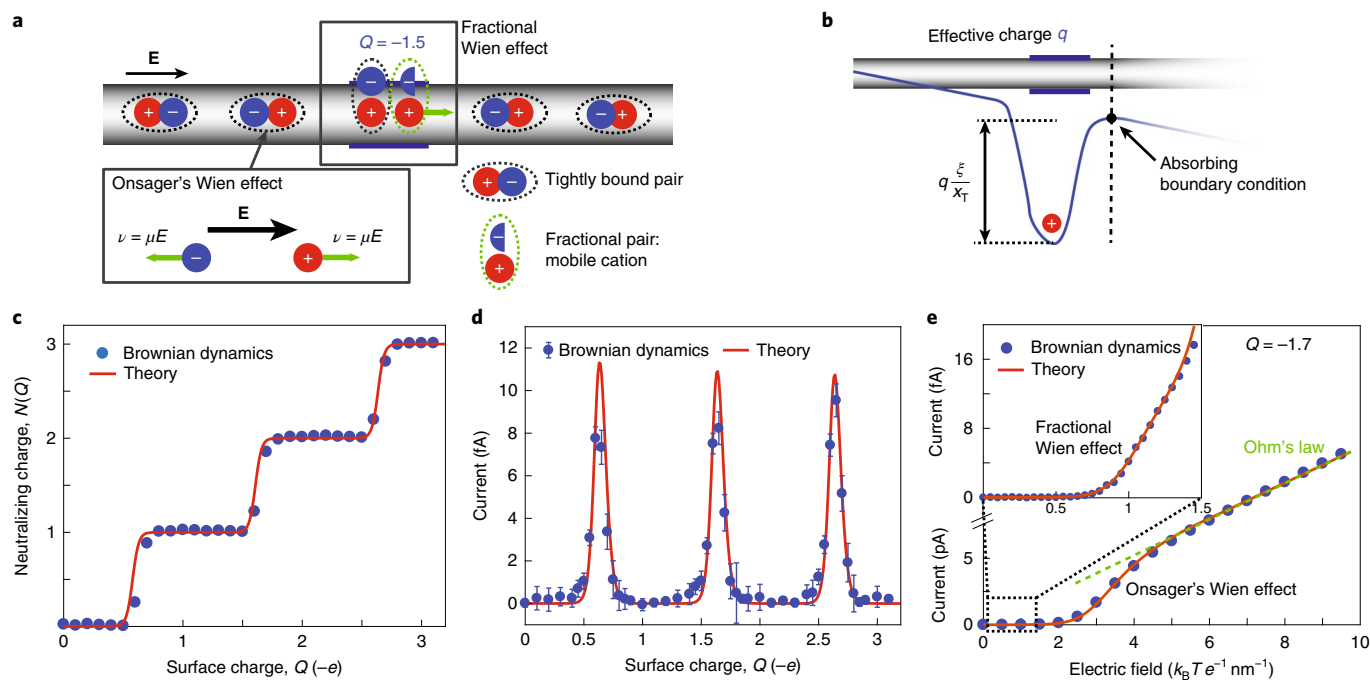


Fig. 2 | Analytical theory for the fractional Wien effect mechanism of ionic CB. **a**, Schematic representation of Onsager's Wien effect and of the fractional Wien effect. Both correspond to nonlinearities in the current-voltage characteristic due to the electric field dependence of the dissociation rate of ion pairs. **b**, Schematic setting for the study of out-of-equilibrium Bjerrum pair dynamics. The main ingredient is the computation of the mean escape time of an ion from the potential created by an effective charge q . **c**, Neutralizing charge $N(Q)$ as a function of surface charge. **d**, Positive ion current, at fixed applied electric field ($E = 1 k_B T e^{-1} \text{ nm}^{-1}$), as a function of surface charge. **e**, Current-voltage characteristic at fixed surface charge, corresponding to a conductance peak ($Q = -1.7$). Inset, enlarged view of the region of small applied electric field. In **c–e**, dots are simulation results, while the solid line is the theoretical prediction from equations (5) and (8). The Wien effect theory shows quantitative agreement with simulations. Error bars represent the standard deviation of the mean.

with the initial condition $\mathcal{P}(\phi, 0 | \phi_0) = \delta(\phi - \phi_0)$ and where $z = e^{\beta\mu}$ is the fugacity.

This result allows us to unveil the unconventional behaviour of the ionic system. As a first indication, the equation of state of the confined ionic gas can be exactly derived in the limit $z_T \equiv zx_T/L \ll 1$, corresponding to strong electrostatic interactions (with our simulation settings, $z_T = 0.02$), yielding

$$P = \frac{1}{2} \rho k_B T \cdot (1 + O(z_T^2)) \quad (4)$$

where P is the pressure and ρ is the salt density (Supplementary Section 1.10). Thus, when the interactions are strong enough, the ionic gas of density ρ behaves as an ideal gas of density $\rho/2$. This means that ions of opposite charge are actually bound together in the form of Bjerrum pairs, as confirmed by direct observation in the simulations (Supplementary Video 1). The confined salt behaves accordingly as a weak electrolyte. We will now demonstrate that this crucial characteristic, missed by mean-field theory, is key to explaining both the conductance gating and the strongly nonlinear response under an electric field, as highlighted in Fig. 1.

Let us first sketch a qualitative picture. In a weak electrolyte, the conduction should proceed through the second Wien effect, which was famously explained by Onsager^{33,34}. In Onsager's picture, tightly bound ion pairs cannot move under the effect of an electric field, and current can only flow when an ion pair dissociates (Fig. 2a). This picture applies to our system, except for the presence of the gating charge Q , which acts as a 'defect' and affects the dissociation process of ion pairs. If Q is an integer, all the ions are tightly bound at low enough E and the conductance is vanishing. Now if

Q has a fractional part, it still binds an integer number of ions, so one of those ions may be less strongly bound than the others (for example, if a charge $Q = -1.5$ binds two positive ions). This weakly bound ion may then dissociate from the surface charge under the effect of the external electric field, resulting in non-zero conduction. This qualitative picture is confirmed by direct observation in the simulations (Supplementary Video 1). Interestingly, once a pair dissociates, conduction occurs via a Grotthus-like mechanism, with the free ion exchanging between Bjerrum pairs. Altogether, the conduction is due to ions dissociating not from their opposite charge counterparts, but from the fractional surface charge: we thus name this new mechanism the 'fractional Wien effect'.

In addition to the surface charge gating, the fractional Wien effect picture allows us to understand the nonlinear current-voltage characteristics. Indeed, at low electric fields, the conduction is due to the dissociation of fractional ion-surface charge pairs, whose dissociation rate depends on the electric field, thus the conductance acquires an electric field dependence. However, at sufficiently high electric fields, the Bjerrum pairs that are present in the bulk of the channel will also start dissociating, resulting in the standard ('bulk') Wien effect that was studied by Onsager. This results in another nonlinearity in the $I-V$ curve, before a collapse into Ohm's law once all the pairs have been dissociated.

We now develop an out-of-equilibrium framework to quantify the fractional Wien picture that has emerged. As a first step, the exact solution (2) for the partition function Ξ allows us to compute the probability of the system containing a fractional ion-surface charge pair, or equivalently the average neutralizing charge $N(Q)$. In the limit of an infinite channel and a point-like surface charge, we obtain $N(Q) = -(x_T/\xi)(\partial \log \Xi / \partial Q) - Q$, and a lengthy calculation

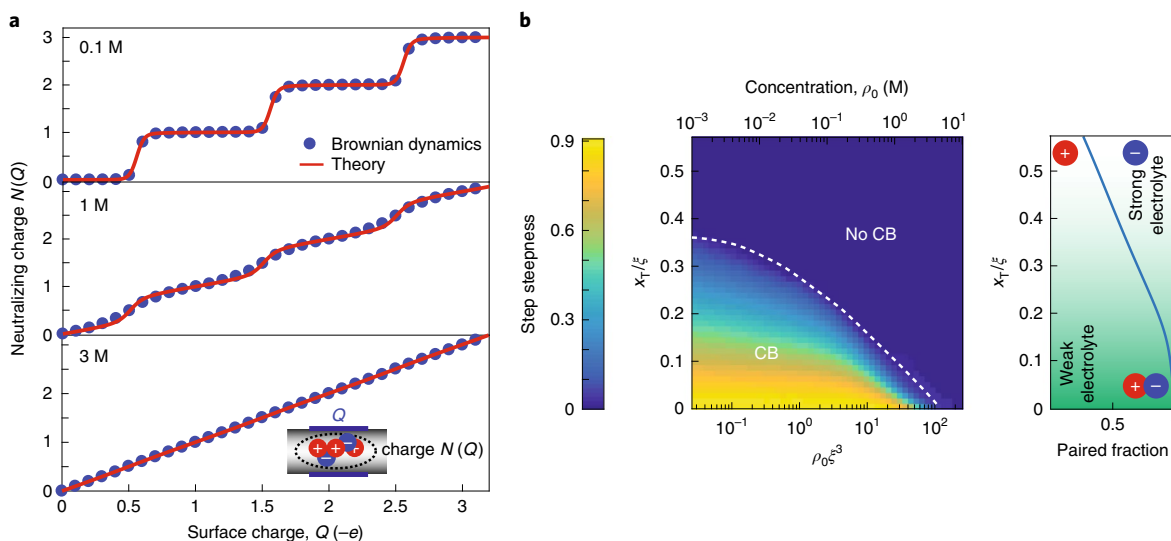


Fig. 3 | Conditions for observation of ionic CB. **a**, Neutralizing charge $N(Q)$ as a function of the surface charge Q , as obtained from Brownian dynamics simulations (dots) and the full theoretical prediction from Supplementary equation (32) (solid line), at different salt concentrations c . CB steps disappear as the salt concentration is increased. The parameters are chosen here as $x_T = 0.18$ nm and $\xi = 7$ nm. **b**, ‘Phase diagram’ for CB. The colour scale shows, as an assessment of the ‘strength’ of ionic CB, the steepness of the steps in the neutralizing charge $N(Q)$. It is defined as $1 - 1/\text{maximum slope of a step}$ and varies between 0 (no CB) and 1 (full CB). The axes correspond to the channel radius (in terms of the dimensionless quantity $x_T/\xi = R^2/2\ell_B\xi$) and to the dimensionless bulk salt concentration $\rho_0\xi^3$. On the right panel, the fraction of ion pairs in the channel is plotted as a function of x_T/ξ , at bulk concentration 0.1M. Ion pairing is a prerequisite for ionic CB; that is, CB occurs when the salt behaves as a weak electrolyte.

(reported in Supplementary Section 1.9) yields an analytical expression, which can be written in the form

$$N(Q) = \frac{\sum_{ij} a_i a_j (j-i) e^{-\frac{\xi}{2x_T}(Q-(i-j))^2}}{\sum_{ij} a_i a_j e^{-\frac{\xi}{2x_T}(Q-(i-j))^2}} - Q \quad (5)$$

(see Supplementary equation (35) for an exact expression). Coefficients a_i are obtained as series expansions in $z_T \equiv x_T/L$ (a few terms are sufficient in the limit of interest $z_T \ll 1$). The prediction in equation (5) is plotted in Fig. 2c: it accounts for a quantized neutralizing charge, and the agreement with simulations is excellent. Assuming strong enough interactions, one may adopt a ‘two-state’ perspective: the surface charge Q may bind either $\lfloor Q \rfloor$ or $\lfloor Q \rfloor + 1$ counterions ($\lfloor \cdot \rfloor$ denotes the floor function). In the latter case, a fractional ion–surface charge pair is formed. The probability of the system containing this weakly bound pair is accordingly $p(Q) = N(Q) - \lfloor Q \rfloor$.

In a second step, we study the out-of-equilibrium dynamics of a Bjerrum pair. We consider a single ion bound to an effective charge q (Fig. 2b). Its probability distribution $P(x, t)$ is governed by the Fokker–Planck equation

$$\partial_t P = D \partial_x (P \partial_x [-qV(x) - Ex]) + D \partial_x^2 P \quad (6)$$

where D is the diffusion coefficient, E the applied electric field and $V(x)$ the pairwise interaction potential in equation (1). Solving equation (6) with an absorbing boundary condition (Fig. 2b) yields the mean escape time for the bound ion (see Supplementary Section 2.1 and ref. 35):

$$\tau(q, E) = \frac{1}{D} \int_{-\infty}^{+\infty} \int_{\max(0, x)}^{\xi \log \frac{q}{Ex_T}} e^{q(V(x) - V(y)) + E(x-y)} dy dx \quad (7)$$

For a bulk ion pair the effective charge q is 1, and the average lifetime of the pair is actually $\tau(1, E)/2$ because both ions are mobile; for

a fractional ion–surface charge pair, $q = Q - \lfloor Q \rfloor$. In Supplementary Section 2.2 we derive the relationship between the lifetime of the ion pairs and the number of free charge carriers. Combining this result with the probability $p(Q)$ of finding a weakly bound pair in the system yields an expression for the positive ion current $I^+(E)$ accounting for both the fractional and the bulk Wien effect:

$$I^+(E) = (N(Q) - \lfloor Q \rfloor) I_{Q - \lfloor Q \rfloor}(E) + I_{\text{bulk}}^+(E) \quad (8)$$

with $I_q(E) = (L/(DE) + \tau(q, E))^{-1}$ and

$$I_{\text{bulk}}^+(E) = \frac{1}{2\tau(1, E)} (\sqrt{1 + 2\rho DE\tau(1, E)} - 1)$$

These analytical predictions for the current (equation (8)) are plotted in Fig. 2d,e and reproduce quantitatively the simulation results. Our result accounts both for the CB oscillations—enhanced conductance at quantized values of surface charge—and for the ‘blockade’ of ionic transport in the form of the strongly nonlinear current voltage relation at low applied field. The theory fully validates the fractional Wien mechanism, highlighting that this effect originates in an interplay between many-body dynamics of ion pairs and Coulomb gas statistics.

Phase diagram

Having now established a theoretical framework for ionic CB that is quantitatively validated against molecular simulations, we may use it to obtain insight into the conditions under which one may expect ionic CB. Figure 3a shows the prediction for the neutralizing charge $N(Q)$ at increasing salt concentrations: strikingly, the CB steps disappear at high salt concentration as a result of Debye screening, again in full agreement with simulations. This is a crucial specificity of our ionic system with respect to its electronic counterpart. Going further, we build a phase diagram that displays the parameter space where ionic CB occurs (that is, where $N(Q)$ versus Q displays steps) in terms of dimensionless ion density and channel size (Fig. 3b). Ionic CB indeed disappears above a critical salt concentration

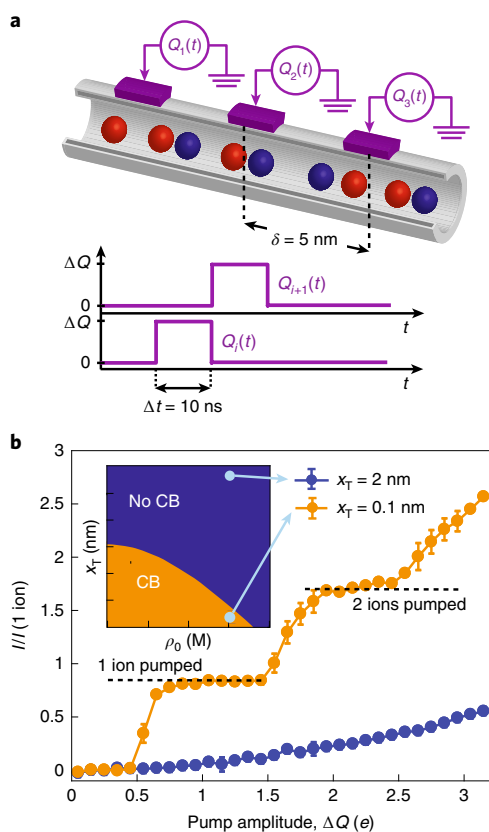


Fig. 4 | Ionic-CB-based ion pump. **a**, Schematic of the ion pump inspired by its electronic counterpart and time dependence of the variable surface charges $Q_i(t)$. The 125 variable charges are placed every 5 nm, and periodic boundary conditions are used. **b**, Positive ion current resulting from the pump operation (with no applied electric field), at $x_T = 0.1$ nm (CB regime) and $x_T = 2$ nm (no CB), as obtained from Brownian dynamics, as a function of the pump amplitude ΔQ . The current is normalized by $I(1 \text{ ion})$, which is the current resulting from one ion moving at a velocity of 5 nm per 10 ns. Error bars represent the standard deviation of the mean.

for a given channel size (or x_T); Debye screening thus does prevent CB, though only at rather high salt concentration values (typically, more than 2 M for a 1 nm channel). Conversely, at a given salt concentration, a small enough x_T (strong enough interactions) is required for ionic CB to occur. In the limit $z_T \ll 1$, the slope of a step is given by $(dN/dQ)_{\max} = \xi/(4x_T) + O(z_T^4)$ (Supplementary Section 1.9). Therefore a necessary condition for observing steps is $\xi/x_T \gtrsim 4$, that is the Coulomb interaction between two ions should be greater than $\sim 4k_B T$. Concretely, this corresponds to nanochannel sizes $R \lesssim 3.5\ell_B \sim 2.5$ nm for monovalent ions. For multivalent ions with valency p , the Bjerrum length increases as p^2 and this modifies accordingly the condition on the channel size. Thus, our theory demonstrates that ionic CB can actually be expected in channels that are much larger than previously considered biological nanopores^{21,22} of radius $R \approx 0.3$ nm. Finally, the right panel of Fig. 3b shows the fraction of Bjerrum pairs as predicted by our theory (Supplementary Section 1.11): it decreases with increasing x_T , in line with the disappearance of CB steps, highlighting once more that ionic CB and Bjerrum pairing are intimately related.

Ion pump

Our modelling of ionic CB opens the way to the design of new functionalities in nanofluidic systems. Beyond gated transport itself, one may also harness the control over single ions allowed by CB to

develop ion pumping functionalities. Single electron pumps have been obtained by associating two CB devices in series, with their gate voltages oscillating out of phase³⁶. Figure 4a shows an analogous ionic system, a nanochannel with variable surface charges placed along its length. We confirm using Brownian dynamics simulations that such a device is capable of pumping activity. With appropriate modulation of the surface charges, and in the absence of applied electric field, there is indeed transport of ions along the channel; the modulation amplitude ΔQ allows us to precisely control the discrete number of ions being transported (Fig. 4b). Most importantly, however, the simulations highlight that the pumping fully relies on the system operating in the CB regime. Indeed, the pumping current is almost 0 at large x_T (weak interactions, no CB), while it is significant only at small x_T (strong interactions, CB regime; see inset of Fig. 4b). This proof of concept confirms the importance of ionic CB as a building block for artificial devices mimicking biological functions; we leave to future work the thorough investigation of such devices.

Conclusions

Thanks to a many-body framework for the non-equilibrium ion dynamics—far beyond the mean field approximation—we unveil the subtle physical mechanisms underlying the ionic equivalent of CB in a general nanochannel geometry. We highlight that, in stark contrast to its electronic counterpart, ionic CB in a nanochannel relies on the Bjerrum pairing of ions and a fractional Wien-effect mechanism. Building on this fundamental result, we are able to provide a theoretical benchmark for the experimental realization of ionic CB, establishing prerequisite conditions in terms of confinement and salt concentration, as summarized in the phase diagram in Fig. 3b. Ionic CB requires nanometric confinement for monovalent ions, but this condition is strongly mitigated for multivalent species. These estimates are impacted by the dielectric properties of water in strong confinement; although we propose a way to account for the anisotropic permittivity of confined water^{25,26}, additional insight from simulations or experiments is needed to precisely evaluate the interactions at such scales. Finally, beyond the 1D systems considered here, the recently developed 2D ion channels based on van der Waals heterostructures could also exhibit CB-like behaviour, with the weaker 2D interactions potentially compensated by the very low permittivity observed in these channels²⁶. The exploration of ionic CB in these systems is already within reach, opening exciting perspectives for the development of advanced ionic machinery.

Data availability

The data that support the plots within this paper and other findings of this study are available from the corresponding authors upon reasonable request.

Code availability

The Brownian dynamics code used within this study is available from the corresponding authors upon reasonable request.

Received: 18 September 2018; Accepted: 7 March 2019;

Published online: 08 April 2019

References

- Schoch, R. B., Han, J. & Renaud, P. Transport phenomena in nanofluidics. *Rev. Mod. Phys.* **80**, 839 (2008).
- Bocquet, L. & Charlaix, E. Nanofluidics, from bulk to interfaces. *Chem. Soc. Rev.* **39**, 1073–1095 (2010).
- Elimelech, M. & Phillip, W. A. The future of seawater desalination: energy, technology and the environment. *Science* **333**, 712–717 (2011).
- Lauger, P. Mechanisms of biological ion transport—carriers, channels and pumps in artificial lipid membranes. *Angew. Chem. Int. Ed.* **24**, 905–923 (1985).
- Apell, H. J. & Karlisch, S. J. Functional properties of Na,K-ATPase, and their structural implications, as detected with biophysical techniques. *J. Membr. Biol.* **180**, 1–9 (2001).

6. Heginbotham, L., Kolmakova-Partensky, L. & Miller, C. Functional reconstitution of a prokaryotic K⁺ channel. *J. Gen. Physiol.* **111**, 741–749 (1998).
7. Dayan, P. *Theoretical Neuroscience* (MIT Press, 2000).
8. Siria, A. et al. Giant osmotic energy conversion measured in a single transmembrane boron nitride nanotube. *Nature* **494**, 455–458 (2013).
9. Radha, B. et al. Molecular transport through capillaries made with atomic-scale precision. *Nature* **538**, 222–225 (2016).
10. Feng, J. et al. Single-layer MoS₂ nanopores as nanopower generators. *Nature* **536**, 197–200 (2016).
11. Tunuguntla, R. H. et al. Enhanced water permeability and tunable ion selectivity in subnanometer carbon nanotube porins. *Science* **357**, 792–796 (2017).
12. Nazarov, Y. V. & Blanter, Y. M. *Quantum Transport: Introduction to Nanoscience* (Cambridge Univ. Press, 2009).
13. Beenakker, C. W. J. Theory of Coulomb-blockade oscillations in the conductance of a quantum dot. *Phys. Rev. B* **44**, 1646–1656 (1991).
14. Stopa, M. Rectifying behavior in Coulomb blockades: charging rectifiers. *Phys. Rev. Lett.* **88**, 146802 (2002).
15. Krems, M. & Di Ventra, M. Ionic Coulomb blockade in nanopores. *J. Phys. Condens. Matter* **25**, 065101 (2013).
16. Tanaka, H., Iizuka, H., Pershin, Y. V. & Di Ventra, M. Surface effects on ionic Coulomb blockade in nanometer-size pores. *Nanotechnology* **29**, 025703 (2017).
17. Li, W. et al. Gated water transport through graphene nanochannels: from ionic Coulomb blockade to electroosmotic pump. *J. Phys. Chem. C* **121**, 17523–17529 (2017).
18. Feng, J. et al. Observation of ionic Coulomb blockade in nanopores. *Nat. Mater.* **15**, 850–855 (2016).
19. Kaufman, I. K. et al. Ionic Coulomb blockade and anomalous mole fraction effect in the NaChBac bacterial ion channel and its charge-varied mutants. *EPJ Nonlinear Biomed. Phys.* **5**, 4 (2017).
20. Fedorenko, O. A. et al. Quantized dehydration and the determinants of selectivity in the NaChBac bacterial sodium channel. Preprint at <https://arxiv.org/abs/1803.07063> (2018).
21. Kaufman, I., Luchinsky, D. G., Tindjong, R., McClintock, P. V. E. & Eisenberg, R. S. Multi-ion conduction bands in a simple model of calcium ion channels. *Phys. Biol.* **10**, 026007 (2012).
22. Kaufman, I. K., McClintock, P. V. E. & Eisenberg, R. S. Coulomb blockade model of permeation and selectivity in biological ion channels. *New J. Phys.* **17**, 083021 (2015).
23. von Kitzing, E. in *Membrane Proteins: Structures, Interactions and Models* (eds Pullman, A., Jortner, J. & Pullman, B.) 297–314 (Springer, 1992).
24. Luchinsky, D. G., Gibby, W. A. T., Kaufman, I., Timucin, D. A. & McClintock, P. V. E. Statistical theory of selectivity and conductivity in biological channels. Preprint at <https://arxiv.org/abs/1604.05758> (2016).
25. Schlaich, A., Knapp, E. W. & Netz, R. R. Water dielectric effects in planar confinement. *Phys. Rev. Lett.* **117**, 048001 (2016).
26. Fumagalli, L. et al. Anomalously low dielectric constant of confined water. *Science* **360**, 1339–1342 (2018).
27. Zhang, J., Kamenev, A. & Shklovskii, B. I. Conductance of ion channels and nanopores with charged walls: a toy model. *Phys. Rev. Lett.* **95**, 148101 (2005).
28. Zhang, J., Kamenev, A. & Shklovskii, B. I. Ion exchange phase transitions in water-filled channels with charged walls. *Phys. Rev. E* **73**, 051205 (2006).
29. Cooper, K., Jakobsson, E. & Wolynes, P. The theory of ion transport through membrane channels. *Prog. Biophys. Mol. Biol.* **46**, 51–96 (1985).
30. Edwards, S. F. & Lenard, A. Exact statistical mechanics of a one-dimensional system with Coulomb forces. II. The method of functional integration. *J. Math. Phys.* **3**, 778–792 (1962).
31. Démary, V., Dean, D. S., Hammant, T. C., Horgan, R. R. & Podgornik, R. The one-dimensional Coulomb lattice fluid capacitor. *J. Chem. Phys.* **137**, 064901 (2012).
32. Kamenev, A., Zhang, J., Larkin, A. I. & Shklovskii, B. I. Transport in one-dimensional Coulomb gases: from ion channels to nanopores. *Physica A* **359**, 129–161 (2006).
33. Onsager, L. Deviations from Ohm's law in weak electrolytes. *J. Chem. Phys.* **2**, 599–615 (1934).
34. Kaiser, V., Bramwell, S. T., Holdsworth, P. C. W. & Moessner, R. Onsager's Wien effect on a lattice. *Nat. Mater.* **12**, 1033–1037 (2013).
35. Redner, S. *A Guide to First Passage Problems* (Cambridge Univ. Press, 2001).
36. Pothier, H., Lafarge, P., Urbina, C., Esteve, D. & Devoret, M. H. Single-electron pump based on charging effects. *Eur. Phys. Lett.* **17**, 249–254 (1992).

Acknowledgements

The authors thank V. Démary, R. Vuilleumier, B. Rotenberg, D. Dean, R. Netz, A. Poggioli, T. Mouterde, L. Jubin and H. Yoshida for useful discussions. S.M. and L.B. acknowledge support from ANR Neptune. L.B. acknowledges support from ERC, project Shadoks, and European Union's H2020 Framework Programme/FET NanoPhlow. This work was granted access to the HPC resources of MesoPSL financed by the Region Ile de France and the project Equip@Meso (reference ANR-10-EQPX-29-01) of the programme Investissements d'Avenir supervised by the Agence Nationale pour la Recherche, as well as to the HPC resources of CINES under allocation 2018-A0040710395 made by GENCI.

Author contributions

L.B. and A.S. conceived the project. N.K. carried out the theoretical analysis and Brownian dynamics simulations. N.K. and L.B. co-wrote the paper. All authors discussed the results and commented on the manuscript.

Competing interests

The authors declare no competing interests.

Additional information

Supplementary information is available for this paper at <https://doi.org/10.1038/s41565-019-0425-y>.

Reprints and permissions information is available at www.nature.com/reprints.

Correspondence and requests for materials should be addressed to L.B.

Journal peer review information: *Nature Nanotechnology* thanks Peter (V. E.) McClintock, Aleksandra Radenovic and the other anonymous reviewer(s) for their contribution to the peer review of this work.

Publisher's note: Springer Nature remains neutral with regard to jurisdictional claims in published maps and institutional affiliations.

© The Author(s), under exclusive licence to Springer Nature Limited 2019